Article

Determination and measurement of melanopic equivalent daylight (D65) illuminance (*mEDI*) in the context of smart and integrative lighting

Vinh Quang Trinh [1]*, Peter Bodrogi [2], and Tran Quoc Khanh [1]

[1] Laboratory of Adaptive Lighting Systems and Visual Processing, Technical University of Darmstadt, Hochschulstr. 4a, 64289 Darmstadt, Germany; vinh@lichttechnik.tu-darmstadt.de (V.Q.T.); khanh@lichttechnik.tu-darmstadt.de (T.Q.K.).
[2] ERCO GmbH, Brockhauser Weg 80-82, Lüdenscheid, Germany; p.bodrogi@erco.com (P.B.);
* Correspondence: vinh@lichttechnik.tu-darmstadt.de; Tel.: +49 6151 16-22881

Abstract: In the context of intelligent and integrative lighting, in addition to the need for color quality and brightness, the non-visual effect is essential. This refers to the retinal ganglion cells (*ipRGCs*) and their function, first proposed in 1927. The melanopsin action spectrum has been published in CIE S 026/E: 2018 [1] with the corresponding melanopic equivalent daylight (D65) illuminance (*mEDI*), melanopic daylight (D65) efficacy ratio (*mDER*) and 4 other parameters. Due to the importance of *mEDI* and *mDER*, this work synthesizes a simple computational model of *mDER* as the main research objective, based on a database of 4214 practical spectral power distributions (SPDs) of daylight, conventional, LED, and mixed light sources. In addition to the high correlation coefficient R^2 of 0.96795 and the 97% confidence offset of 0.0067802, the feasibility of the *mDER* model in intelligent and integrated lighting applications has been extensively tested and validated. The uncertainty between the *mEDI* calculated directly from the spectra and that obtained by processing the RGB sensor and applying the *mDER* model has reached ± 3.3% after an appropriate matrixing process and proper illumination characterization combined with the successful *mDER* calculation model. This result opens the potential of low-cost RGB sensors for applications in intelligent and integrative lighting systems to optimize and compensate the non-visual effective parameter *mEDI* using daylight and artificial light in indoor spaces. The goal of the research on *RGB* sensors and the corresponding processing method are also presented and their feasibility is methodically demonstrated. A comprehensive investigation with a huge amount of color sensor sensitivities is necessary in a future work of other researches.

Keywords: Non-visual effects of light, Melanopic equivalent daylight (D65) illuminance, *mEDI*, Melanopic equivalent daylight (D65) efficacy ratio, *mDER*, Intelligent and integrated lighting, *mDER* calculation model, *mEDI* measurement, *mEDI* determination

1. Introduction

The development of lighting technology from the beginning of the 20^{th} century to the present can be roughly divided into three stages, some of which overlap. Until the end of the 20^{th} century, with thermal radiators and discharge lamps as light sources, the first component of integrative HCL ("*Human Centric Lighting*") lighting technology was about "*visual performance*" (e.g. reaction time, contrast perception, reading speed, visual acuity) to enable visibility, improve work performance and minimize error rates in industrial processes, educational and healthcare facilities and offices, among others [2–10]. Since the 1970s and even more so since the mid-1990s, with the growing importance of education and the information society, the psychological effects of light (e.g. scene preference, room preference, user satisfaction, spatial perception, attractiveness and color preference) have become more and more important. Recent results of lighting, color and visual perception research lead to the results in Table 1 [10–17].

Preprints (www.preprints.org) | NOT PEER-REVIEWED | Posted: 6 April 2023 doi:10.20944/preprints202304.0087.v1

Table 1: Recommended parameters for interior lighting in [10–17]

No.	Parameter	Preferred values
1	Horizontal illuminance $E_{v,h}$ in lux [12–14]	Greater than 850 lx; Recommended range: 1300 lx – 1500 lx
2	Correlated color temperature CCT in K [15,16]	4000 K - 5000 K
3	Color rendering index $CIE\ CRI$ [10]	> 80
4	Indirect to total illuminance ratio γ[11,17]	> 0.6 - 0.8

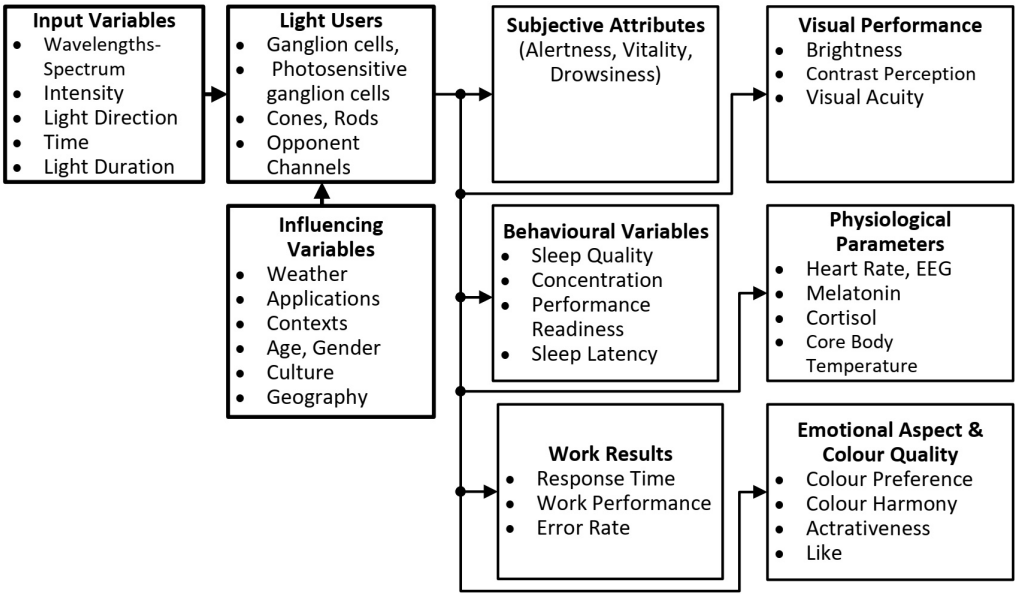

Figure 1. Input variables, influencing factors and output variables in a comprehensive view of the effects of light on humans.

Since the beginning of the 21^{st} century with the quantitative discovery of intrinsically photosensitive retinal ganglion cells (ipRGCs), other non-visual effects of light have been considered, such as circadian rhythm, hormone production and suppression, sleep quality, alertness, and mood. The overall picture of light effects on humans in the three contexts of "*visual performance*", "*psychological light effects*" and "*non-visual light effects*" is shown in Figure 1, attempting to describe a chain of signal processing from the optical and temporal input parameters to the light users with influencing parameters to the output parameters expressing the physiological, behavioral and human biological effects of light and lighting.

In recent years, there has been a large amount of research and publications on non-visual lighting effects analyzed and reviewed in books and literature reviews [18–21]. In the majority of scientific publications cited in these reviews, the input parameters describing lighting conditions were photometric metrics (illuminance, luminance) and/or color temperature. In addition to the optimal lighting design of buildings and the development of modern luminaires according to the criteria of visual performance and psychological lighting effects, it is necessary to define suitable input parameters for the description of non-visual lighting effects, to determine their optimal values and to measure these parameters in a wide variety of applications in the laboratory and in the field. To achieve the above goal, the following three research questions for lighting research must be formulated in general terms:

1. Which input parameters can be used to describe the non-visual effects of light in their variety of manifestations (alertness, sleep quality, hormone production and suppression, phase shift)?

 doi:10.20944/preprints202304.0087.v1

2. What values of these input variables are currently considered in the literature to be minimum, maximum, or optimal?
3. Which measuring devices, sensor systems and measuring methods can be used to measure the input quantities for the non-visual lighting effects and process them in the context of smart lighting in the course of the control and regulation of LED or OLED luminaires on the basis of the definition of personal and room-specific applications?

To define the parameters of non-visual lighting effects (Research Question 1), the International Commission on Illumination (*CIE*) and scientists in the fields of neurophysiology, sleep research, and lighting technology have recently made efforts to find effective parameters based on the evaluation of the five photoreceptor signals (*LMS* cones, rods, and *ipRGC* cells) and the corresponding calculation tool [22]. This scientific process resulted in the definitions of "*Melanopic Equivalent Daylight (D65) Illuminance (mEDI)*" and "*Melanopic Daylight (D65) Efficacy Ratio (mDER)*". These definitions have been recognized and used by international experts for several years and form the basis of Section 2 of this paper.

To answer Research Question 2, recognized international sleep researchers and neuroscientists in 2022 made some recommendations regarding non-visual light effects, physiological aspects, sleep and wakefulness based on their literature reviews [23]. Physiological aspects included hormonal regulation cycles, heart rate, core body temperature, and certain brain activities. The main findings were as follows,

(a) "*Daytime light recommendations for indoor environments: Throughout the daytime, the recommended minimum melanopic EDI is 250 lux at the eye measured in the vertical plane at approximately 1.2 m height (i.e., vertical illuminance at eye level when seated)*".
(b) "*Evening light recommendations for residential and other indoor environments: During the evening, starting at least 3 hours before bedtime, the recommended maximum melanopic EDI is 10 lux measured at the eye in the vertical plane approximately 1.2 m height. To help achieve this, where possible, the white light should have a spectrum depleted in short wavelengths close to the peak of the melanopic action spectrum*".
(c) "*Nighttime light recommendations for the sleep environment: The sleep environment should be as dark as possible. The recommended maximum ambient melanopic EDI is 1 lux measured at the eye*".

The first recommendation, with a minimum value of "*melanopic EDI = Melanopic Equivalent Daylight (D65) Illuminance, mEDI*" of 250 lx measured vertically at the observer's eye, is relevant and of great interest for the professional sector during the day (offices, industrial halls, educational and health facilities). The other two recommendations are for the dark hours in the home.

For the solution of Research Question 3 "*Determination and measurement of input parameters for non-visual lighting effects*", which builds the focus of this present paper, two application areas can be targeted:

1. Determination and measurement of non-visual parameters after completion of the new lighting installations and comparison with the specifications of the previous lighting design; or verification of the results of the development of new luminaires for HCL lighting in the lighting laboratory or in the field. For this purpose, absolute spectroradiometers for spectral radiance or spectral irradiance are used to calculate the parameters *mEDI* and *mDER* at different locations in the building. These two non-visual parameters cannot be measured directly with integral colorimeters and illuminance-luminance meters.
2. Control or regulation of modern semiconductor based lights (LED - OLED) and window systems (daylight systems) with the help of sensors in the room (e.g. presence sensors, position sensors, light and color sensors). In order to achieve

Preprints (www.preprints.org) | NOT PEER-REVIEWED | Posted: 6 April 2023 doi:10.20944/preprints202304.0087.v1

a predefined value of non-visual parameters such as $mEDI$ at a specific location in the room (e.g. in the center of the room or at locations further away from the windows), taking into account dynamically changing weather conditions and the whereabouts of the room users, in practice relatively inexpensive but sufficiently accurate optical sensors (RGB sensors) are required. The goal is to obtain not only the target photometric and colorimetric parameters such as illuminance E_v (in lx), chromaticity coordinates (x, y, z) or correlated color temperature (CCT in K), but also the non-visual parameters $mEDI$ and $mDER$. The principle of this Smart Lighting concept using RGB color sensors is illustrated in Figure 2. The methods for measuring non-visual parameters with low-cost but well-qualified RGB color sensors are the content of the sections 3 and 4 and the focus of this paper.

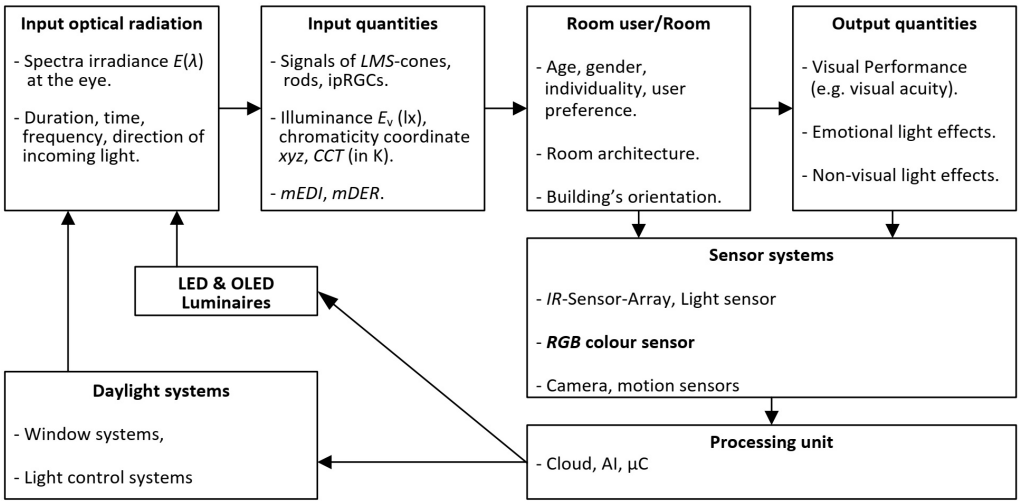

Figure 2. Principle of a Smart Lighting concept with RGB color sensors.

The notations "*integrative lighting*" and "*human-centric-lighting*" used in this publication have been defined by the ISO/CIE publication [24] and mean a lighting concept and practice that integrates both visual and non-visual effects and produces physiological psychological benefits for light users. The terms "*smart lighting*" or "*intelligent lighting*" are used in the same way and mean a framework that combines the above-mentioned integrative lighting as a goal and content of lighting practice with the technological aspects of lighting (signal communication, Internet of Things, sensor systems, control electronics, software including the methods of artificial intelligence, LED luminaires), taking into account the individual needs of light users in dependence on weather conditions, individual human characteristics, time and context of application.

2. Definition of non-visual input parameters [1]

The extensive mathematical treatment and definition of the non-visual input parameters is described in detail in the CIE publication S 026/E:2018 "*CIE System for Metrology of Optical Radiation for ipRGC-Influenced Responses to Light*" [1] and is summarized in this paper. The purpose of this CIE publication is to define spectral response curves, quantities and metrics to describe optical radiation for each of the five photoreceptors in the human eye that may contribute to nonvisual processes. The spectral sensitivity functions of the five receptor types are specified as follows (see Figure 3):

1. S-cone-opic, $s_{10}(\lambda)$
2. M-cone-opic, $m_{10}(\lambda)$
3. L-cone-opic, $l_{10}(\lambda)$
4. Rhodopic, $V'(\lambda)$, rods
5. Melanopic, $mel(\lambda)$, ipRGCs

Preprints (www.preprints.org) | NOT PEER-REVIEWED | Posted: 6 April 2023 doi:10.20944/preprints202304.0087.v1

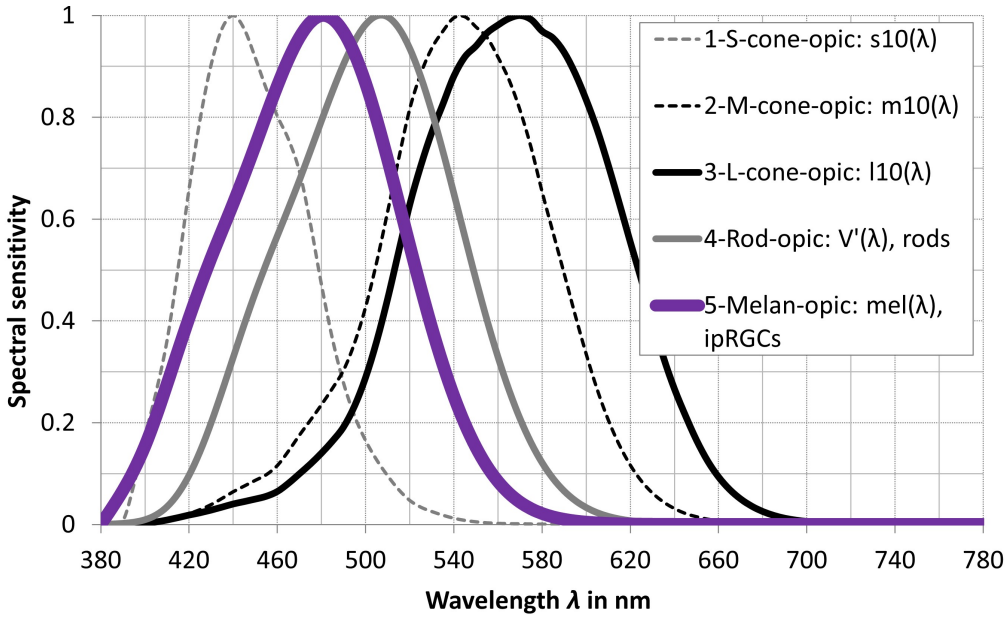

Figure 3. System of relative photoreceptor sensitivities in CIE S 026/E:2018 [1].

The CIE defined the α-opic quantities in Table 2 by the aid of the spectral sensitivities in Figure 3, the spectral radiant flux $\Phi_{e,\lambda}(\lambda)$, the spectral radiance $L_{e,\lambda}(\lambda)$ and the spectral irradiance $E_{e,\lambda}(\lambda)$ (α represents one of the five photoreceptor types).

Table 2: α-opic quantities in CIE S 026/E:2018 [1]

α -opic quantities		
Parameter	Equation	Equation No.
α-opic-radian flux	$\Phi_{e,\alpha}$ or $\Phi_\alpha = \int \Phi_{e,\alpha}(\lambda) \cdot S_\alpha(\lambda) \cdot d\lambda$ (1)	like (3.1) Page 4 [1]
α-opic-radiance	$L_{e,\alpha}$ or $L_\alpha = \int L_{e,\alpha}(\lambda) \cdot S_\alpha(\lambda) \cdot d\lambda$ (2)	like (3.5) Page 4 [1]
α-opic-irradiance	$E_{e,\alpha}$ or $E_\alpha = \int E_{e,\alpha}(\lambda) \cdot S_\alpha(\lambda) \cdot d\lambda$ (3)	like (3.6) Page 5 [1]

From this, further parameters can be derived for assessing the non-visual effect of light, where $S_\alpha(\lambda)$ is the spectral sensitivity function of one of the five receptor types, K_m is the known photometric radiation equivalent (= 683.002 lm/W) and $\Phi_{D65,\lambda}(\lambda)$ is the spectrum of standard daylight type D65, see the equations 4 - 5. The quantity "$K_{\alpha,v}$" is the α-opic - Efficacy of the luminous radiation.

$$K_{\alpha,v} = \frac{\int \Phi_{e,\alpha}(\lambda) \cdot S_\alpha(\lambda) \cdot d\lambda}{K_m \cdot \int \Phi_{e,\alpha}(\lambda) \cdot V_\alpha(\lambda) \cdot d\lambda} \tag{4}$$

Equation 4 is similar to Equation (3.4) on Page 4 of [1].

$$K_{\alpha,v}^{D65} = \frac{\int \Phi_{D65,\alpha}(\lambda) \cdot S_\alpha(\lambda) \cdot d\lambda}{K_m \cdot \int \Phi_{D65,\alpha}(\lambda) \cdot V_\alpha(\lambda) \cdot d\lambda} \tag{5}$$

Equation 5 is similar to Equation (3.7) on Page 5 of [1]. For melanopic efficacy (α = mel), the parameter value $K_{mel,V}^{D65}$ equals 1.3262 mW/lm.

So the parameters $mEDI$ and $mDER$ can be set up as shown in Table 3. If one wants to interpret the meaning of $mEDI$ or $mDER$ for lighting engineering, there are two main aspects:

Preprints (www.preprints.org) | NOT PEER-REVIEWED | Posted: 6 April 2023 doi:10.20944/preprints202304.0087.v1

1. $mEDI$ is the illuminance of the standard daylight illuminant D65 that has as much melanopic efficacy as the test light source for a given illuminance E_v (lx) caused by the test light source, see Equation 6 in Table 3.
2. $mDER$ is the ratio of the illuminance of the standard illuminant D65 ($mEDI$) to the illuminance of the test illuminant E_v (in lx) when the absolute melanopic efficacy of both illuminants is set equal, see Equation 9 in Table 3.

The melanopically effective parameters $mDER$ and $mEDI$ can be calculated from the equations 3, 5, 6 and 9 if the spectral irradiance $E_{e,\lambda}(\lambda)$ is known from a spectroradiometric measurement. The key question in this publication is whether these two parameters can also be determined with sufficient accuracy in practical lighting technology using a well-characterized and inexpensive RGB sensor in the sense of intelligent lighting technology (smart lighting). Section 3 deals with the description of the RGB sensor and how the RGB sensor signals can be transformed into tristimulus values (RGB) and into chromaticity coordinates (xyz) by means of a comprehensive spectral analysis.

Table 3: Melanopic equivalent D65 quantities of CIE S 026/E:2018 [1]

α -opic quantities		
Parameter	Equation	Equation No.
Melanopic Equivalent Daylight (D65) Illuminance ($mEDI$) in lx	$mEDI = \frac{\int_{380}^{780} S_{mel.}(\lambda) \cdot E_{e,\lambda}(\lambda) \cdot d\lambda}{K_{mel.,V}^{D65}}$ (6)	like (3.9) Page 6 [1] with α=mel.
Melanopic daylight (D65) efficacy ratio ($mDER$)	$mDER = \frac{K_{mel.,V}}{K_{mel.,V}^{D65}}(*)$ (7) $mDER = \frac{1}{K_{mel.,V}^{D65}} \cdot \frac{\int_{380}^{780} S_{mel.}(\lambda) \cdot E_{e,\lambda}(\lambda) \cdot d\lambda}{E_v}$ (8) $mDER = \frac{\frac{1}{K_{mel.,V}^{D65}} \cdot \int_{380}^{780} S_{mel.}(\lambda) \cdot E_{e,\lambda}(\lambda) \cdot d\lambda}{E_v}$ (9)	↓ ↓ like (3.10) Page 7 [1] with α=mel.
(*) Note: For the parameter K_x^y (indices x, y according to the corresponding definitions), see Equation 4 and Euation 5 when α = mel. and apply Equation 3 when the calculated parameter is the mel-opic irradiance.		

3. RGB color sensors: Characterization and Signal transformation

After the definition of the non-visual input parameters [1] in Section 2, we can understand the main concepts and mathematical forms of $mEDI$ and $mEDR$. In Section 4, the prediction of a simple computational model of the non-visual quantities $mEDI$ and $mDER$ will be carried out, as well as the verification of the feasibility of a RGB sensor using this model will be implemented to check the synthesized prediction model for lighting applications. And it is also to confirm that the model is not only in the mathematical calculations, but can be applied in the lighting systems with low-cost RGB color sensors. Therefore, Section 3 must attempt to describe RGB color sensors, their characterization, and appropriate signal transformation techniques. This section serves as a link between Section 2 and Section 4, as well as to balance the essential material for the verification of the prediction model using a color sensor as an example in Section 4 later. As a demonstration of the methodology for processing RGB sensors, it is not necessary to collect all color sensor sensitivities, synthesize and compare them, but the most important thing here is to prove that the methodology can work well in this approach. Consequently, the future work can be implemented more comprehensively for different color sensor families by other researches.

Preprints (www.preprints.org) | NOT PEER-REVIEWED | Posted: 6 April 2023 doi:10.20944/preprints202304.0087.v1

3.1. Characterisation of RGB color sensors

Color sensors (see Figure 4) are arrays of individual sensors or a group of sensors based on semiconductors with silicon as the semiconductor material, most commonly used for the visible spectral range between 380 nm and 780 nm.

In order to generate the corresponding spectral sensitivity curves of the individual

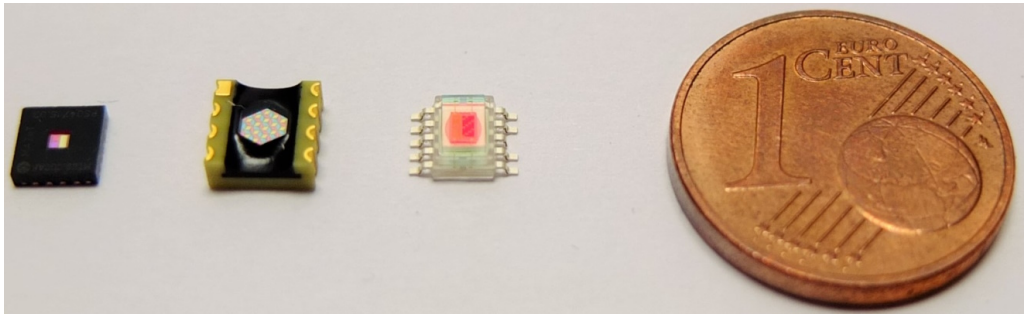

Figure 4. 4 Examples of *RGB* color sensors - From left to right the color sensor chips MTCS-CDCAF, MRGBiCS and S11059 are shown. (Image Source: TU Darmstadt).

color channels in the red, green and blue range (so-called *RGB* . channels), optical color filters based on thin-film technology (interference filters), absorption glass filters or color varnishes are microstructured and applied to the respective silicon sensor. For the correct spatial evaluation of the optical radiation according to the cosine law, a so-called cos prefix (usually a small diffuser plate made of optical scattering materials) is applied to the *RGB* sensor. The photons of each wavelength are absorbed by the *RGB* sensor and photon currents are generated, which are then converted into voltages in an amplifier circuit. These voltages are then digitized in different bit depths (8 bits, 12 bits, 16 bits) by an A/D converter (analog-digital). The spectral sensitivity of each color channel *R* - *G* - *B* is therefore made up of the components shown in the equations 10, 11 and 12.

$$R(\lambda) = S(silicon, \lambda) \cdot \tau(diffusor, \lambda) \cdot \tau(\text{color lacquer}_R, \lambda) \cdot K_R = \frac{CV_R(\lambda)}{E(\lambda)} \tag{10}$$

$$G(\lambda) = S(silicon, \lambda) \cdot \tau(diffusor, \lambda) \cdot \tau(\text{color lacquer}_G, \lambda) \cdot K_G = \frac{CV_G(\lambda)}{E(\lambda)} \tag{11}$$

$$B(\lambda) = S(silicon, \lambda) \cdot \tau(diffusor, \lambda) \cdot \tau(\text{color lacquer}_B, \lambda) \cdot K_B = \frac{CV_B(\lambda)}{E(\lambda)} \tag{12}$$

with,

- $S(silicon, \lambda)$ is the spectral sensitivity of the silicon sensor;
- $\tau(diffusor, \lambda)$ is the spectral transmittance of the cos diffusor;
- $\tau(\text{color lacquer}_i, \lambda)$ is the spectral transmittance of the color filter layer for the respective color channel i = *R*, *G*, *B*;
- K_R, K_G, K_B are absolute factors to account for current-to-voltage conversion and voltage digitization;
- $CV_i(\lambda)$ are output signals (analog or digital) of the respective *R* - *G* - *B* color sensor at wavelength λ.

If a certain spectral irradiance $E(\lambda)$ is present on the *RGB* sensor, three corresponding output signals R, G and B are generated in the three color channels *R*, *G* and *B* (see the equations 13, 14 and 15).

$$R = \int E(\lambda) \cdot R(\lambda) \cdot d\lambda \tag{13}$$

$$G = \int E(\lambda) \cdot G(\lambda) \cdot d\lambda \tag{14}$$

Preprints (www.preprints.org) | NOT PEER-REVIEWED | Posted: 6 April 2023 doi:10.20944/preprints202304.0087.v1

$$B = \int E(\lambda) \cdot B(\lambda) \cdot d\lambda \tag{15}$$

For the calculation of the RGB channel signals it is therefore necessary to know or to determine the spectral sensitivity function of each individual color channel R, G, B by laboratory measurements. The spectral apparatus for determining the spectral sensitivity of the semiconductor sensors in the authors' light laboratory (see Figure 5) therefore consists of a high-intensity xenon ultrahigh-pressure lamp, a grating monochromator (spectral half-width $\Delta\lambda$ = 2 nm, spectral measuring steps for the entire spectrum between 380 nm and 780 nm, $\Delta\lambda$ = 2 nm), and an integrating sphere for homogenizing the quasi-monochromatic radiation coming out of the monochromator. The RGB color sensor and a known calibrated reference sensor are located at two different locations on the inner wall of the sphere behind a shutter.

During the spectral measurement of the RGB sensor, one can determine the spectral sensitivity for the red color channel, for example, according to Equation 16.

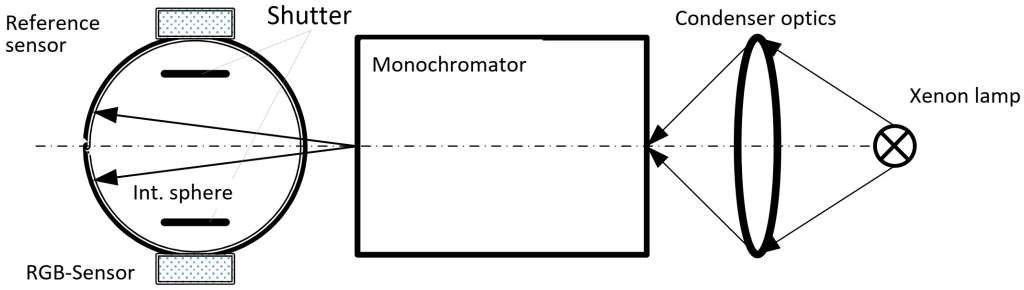

Figure 5. Schematic arrangement for measuring the spectral sensitivity of RGB sensors.

$$R(\lambda) = \frac{CV_R(\lambda)}{E(Sphere, \lambda)} \tag{16}$$

With $CV_R(\lambda)$ as the output signal of the red color channel and $E(\text{sphere}, \lambda)$ as the spectral irradiance at the inner wall of the sphere when the monochromator is set to the wavelength λ, which in turn can be determined from the measured output photocurrent $i(\text{reference}, \lambda)$ and the known spectral sensitivity of the reference sensor $S(reference, \lambda)$, we can write Equation 17.

$$E(\text{sphere}, \lambda) = \frac{i(\text{reference}, \lambda)}{S(\text{reference}, \lambda)} \tag{17}$$

The absolute spectral sensitivity of each color channel R, G, B can be determined from the equations 16 and 17.

Figures 6 and 7 show examples of the spectral response curves of some RGB color sensors measured in the authors' light laboratory. In Figure 6, the two data sets of the same type, SeS1 and SeS2, differ by the different peak heights of the R channel and by the different slopes of the G and B curves, because the two sensors $SeS1$ and $SeS2$ come from different production sets. The $SeS1$ and $SeS2$ spectral sensitivity curves in Figure 6 are fundamentally different from the RGB spectral sensitivity curves of the color sensor type in Figure 7.

3.2. Method of signal transformation from RGB to XYZ

Figure 6 and Figure 7 show that the RGB curves of the real color sensors differ more or less strongly from the xyz curves of the CIE color matching function for a field

Preprints (www.preprints.org) | NOT PEER-REVIEWED | Posted: 6 April 2023 doi:10.20944/preprints202304.0087.v1

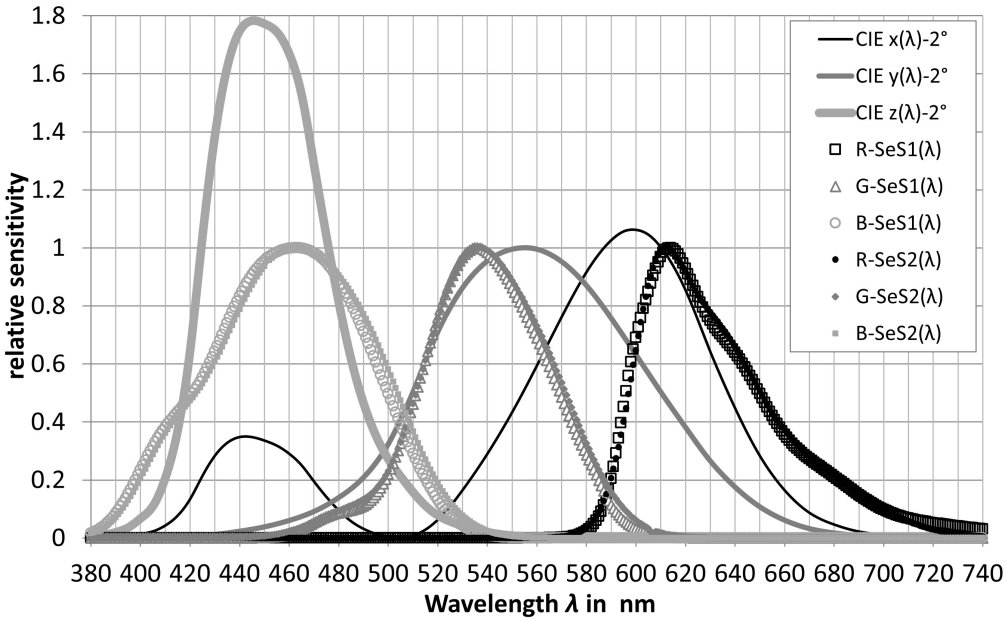

Figure 6. Examples of the spectral sensitivity curves of some *RGB* color sensors.

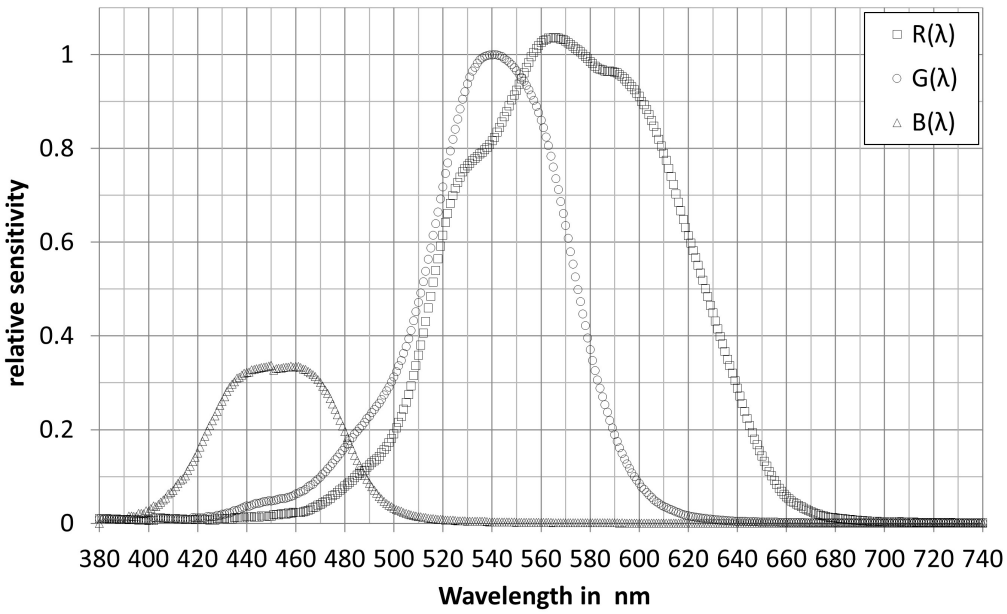

Figure 7. Spectral sensitivity curves of another *RGB* color sensor type.

of view of 2° [25]. In order to obtain the XYZ tristimulus values, the generated RGB signals must be transformed into digital form using matrixing (Equation 18).

$$\begin{pmatrix} X_{SeS,i} \\ Y_{SeS,i} \\ Z_{SeS,i} \end{pmatrix} = \begin{pmatrix} m_{1,1} & m_{1,2} & \dots & m_{1,n} \\ m_{2,1} & m_{2,2} & \dots & m_{2,n} \\ m_{3,1} & m_{3,2} & \dots & m_{3,n} \end{pmatrix} \cdot \begin{pmatrix} R_{1,i} \\ G_{1,i} \\ B_{1,i} \\ \dots \end{pmatrix}. \tag{18}$$

Since the sensor technology, the amplification electronics and the A/D conversion often have a more or less pronounced non-linear behavior, it may be necessary to use different matrixing types from 3 x 3 to 3 x 22, see Table 4.

Preprints (www.preprints.org) | NOT PEER-REVIEWED | Posted: 6 April 2023 doi:10.20944/preprints202304.0087.v1

Table 4: Different matrix types for color sensing according to [26]

Nr.	Size	Content
1	3 x 3	[R G B]
2	3 x 5	[R G B RGB 1]
3	3 x 7	[R G B RG RB GB 1]
4	3 x 8	[R G B RG RB GB RGB 1]
5	3 x 10	[R G B RG RB GB R^2 G^2 B^2 1]
6	3 x 11	[R G B RG RB GB R^2 G^2 B^2 RGB 1]
8	3 x 14	[R G B RG RB GB R^2 G^2 B^2 RGB R^3 G^3 B^3 1]
9	3 x 16	[R G B RG RB GB R^2 G^2 B^2 RGB R^2G G^2B B^2R R^3 G^3 B^3]
10	3 x 17	[R G B RG RB GB R^2 G^2 B^2 RGB R^2G G^2B B^2R R^3 G^3 B^3 1]
11	3 x 19	[R G B RG RB GB R^2 G^2 B^2 RGB R^2G G^2B B^2R R^2B G^2R B^2G R^3 G^3 B^3]
12	3 x 20	[R G B RG RB GB R^2 G^2 B^2 RGB R^2G G^2B B^2R R^2B G^2R B^2G R^3 G^3 B^3 1]
13	3 x 22	[R G B RG RB GB R^2 G^2 B^2 RGB R^2G G^2B B^2R R^2B G^2R B^2G R^3 G^3 B^3 R^2GB RG^2B RGB^2]

If the sensor electronics are linear and the spectral response curves have a similar relative shape to the xyz color matching functions or LMS sensitivity spectra of the retinal photoreceptors, 3 x 3 to 3 x 8 matrices will yield contributions from RGB signals as a function of the first term. The more the sensor electronics deviate from linear behavior and the shape of the spectral curves of the real sensors deviate from the xyz color matching functions, matrices with RGB contributions in quadratic or cubic functions (see Table 4) should be set up. The procedure for finding the optimal matrix based on the chromaticity difference $\Delta u'v'$ is shown in Figure 8.

The goal of the optimization is to get the chromaticity (x, y, z) of the RGB sensor

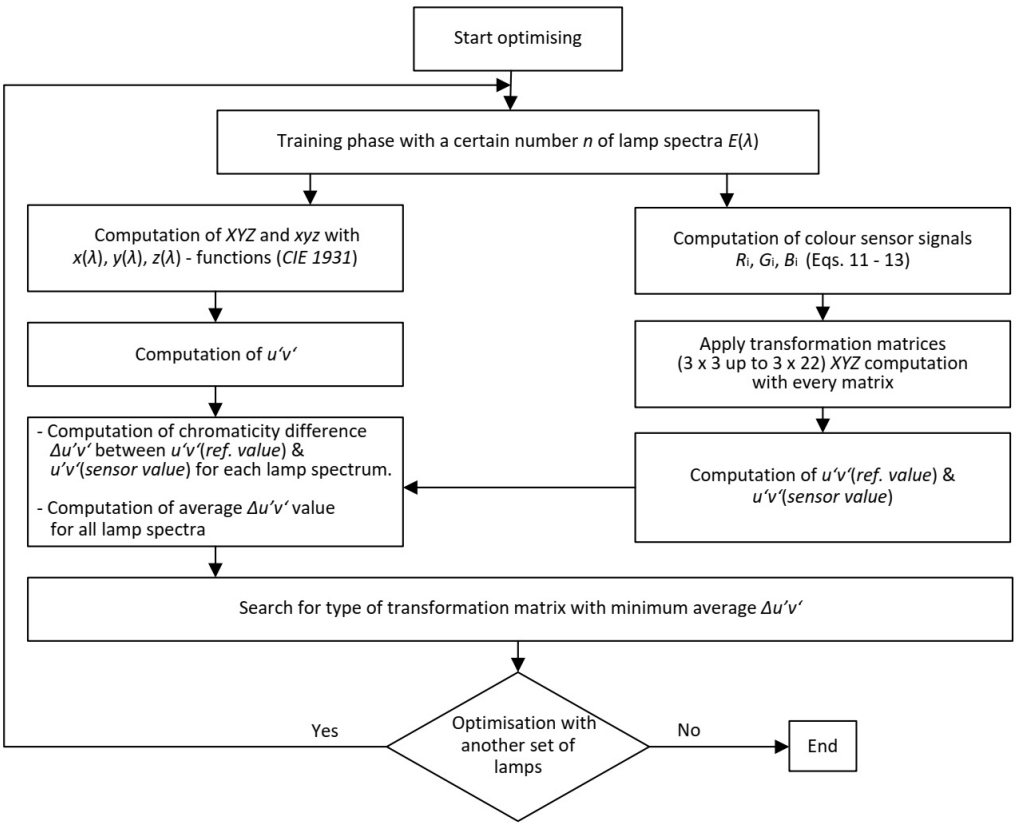

Figure 8. Flowchart of the optimization of a transformation matrix from RGB to XYZ based on the chromaticity difference $\Delta u'v'$ [25].

Preprints (www.preprints.org) | NOT PEER-REVIEWED | Posted: 6 April 2023 doi:10.20944/preprints202304.0087.v1

as close as possible to that derived from the CIE calculation. Instead of working with the non-uniform xy color diagram, it is better to work with the more uniform u'v' diagram (CIE, 1964). Bieske [27] had shown in her dissertation that when $\Delta u'v'$ is less than 10^{-3}, the color difference is not perceived by the subjects. From 10^{-3} to $3 \cdot 10^{-3}$ the color difference can be perceived but is still acceptable. If this value is higher than $5 \cdot 10^{-3}$, the color difference is unacceptable to the subjects. Based on this scientific contribution, the optimization with $u'v'$ not only gives the best z-value, but can also be directly checked and compared with the obtained perception thresholds.

3.3. Matrix transformation in practice, verification with a real RGB color sensor

For the color sensor type whose spectral sensitivity curves are shown in Figure 7, the optimization processes are carried out according to the scheme in Figure 8 with a series of matrix types from 3 x 3 to 3 x 22 with 9 different lamp spectra (as a training set). These nine lamp spectra are tabulated in Table 5 and shown in Figure 9. The illuminance for the optimization of the matrix was chosen to be E_v = 750 lx. In this training set, the following lamp types were selected to reflect the variety of types used in practice today: fluorescent lamps between 2640 K and 4423 K with many spectral lines (see Figure 9), a halogen incandescent lamp, two phosphor-converted white LEDs, and a combination of *RGB* LEDs and warm white LEDs (RGBWW4500K).

Table 5: Properties of the lamp types for matrix optimization

Lamp type	Tungsten halogen	Xenon-2	CFL 3000K	CFL 5000 K	FL 627	FL 645	LED C3L	LED c3N	LED RGBWW4500
CCT (in K)	2762	4100	2640	4423	2785	4423	2640	4580	4500
Duv ($\cdot 10^{-3}$)	3	7.2	0.61	2.2	1.8	2.2	6.3	1.3	-1.0
Ev (in lx)	750	750	750	750	750	750	750	750	750
CIE R9	85	-86	48	-60	-72	-60	-28	-39	36
CIE Ra	97	67	90	68	64	68	67	69	90

The calculation with different matrix types and with individual lamp spectra yields color differences$\Delta u'v'$ of varying magnitude, with the 3 x 3 matrix form yielding the smallest color difference (see Table 6). Optimization with more lamp types did not bring any significant improvement in this case. The final 3 x 3 optimized matrix for the transformation from *RGB* to *XYZ* as well as the formula for the calculation of the illuminance from the *RGB* signals are shown in Table 7.

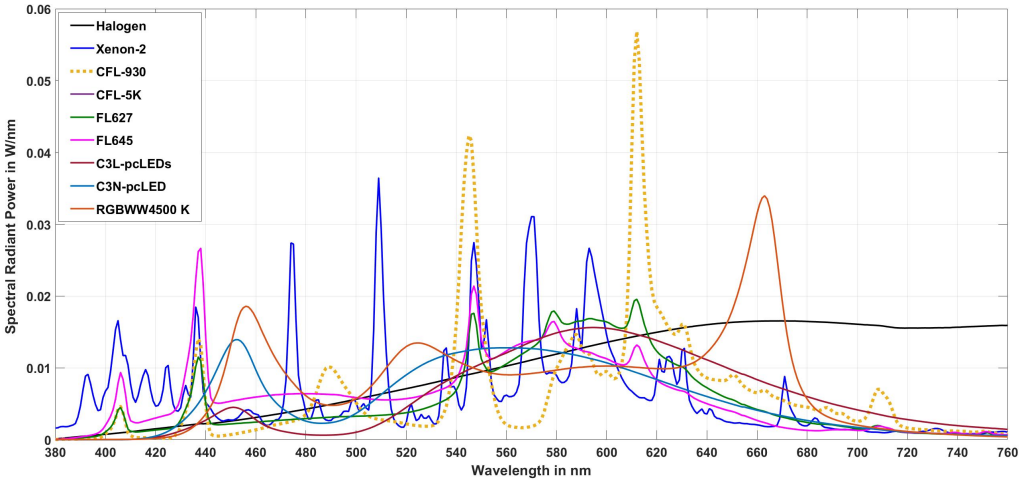

Figure 9. Spectra of the lamp types for matrix optimization.

To verify the prediction quality of the formula in Table 7, 13 lamp spectra were selected in the next step. These were white phosphor converted LEDs (pc-LEDs) and a mixture of daylight spectra with white phosphor converted LEDs (TL-pc-LEDs), as is

Preprints (www.preprints.org) | NOT PEER-REVIEWED | Posted: 6 April 2023 doi:10.20944/preprints202304.0087.v1

Table 6: Chromaticity difference $\Delta u'v'$ for different matrix types for the lamp types of the training set

Name	Xenon-2	CFL-930	CFL-5K	FL627	FL645	C3L-pcLEDs	C3N-pcLED	RGBWW4500 K	Max
$\Delta u'v'_{3x3} \cdot 10^{-3}$	7.4	7.7	1.5	4.5	1.5	0.42	2.7	8.3	8.3
$\Delta u'v'_{3x5} \cdot 10^{-3}$	4.8	48	12	41	12	51	16	16	51
$\Delta u'v'_{3x7} \cdot 10^{-3}$	8.5	5.3	$3.1 \cdot 10^{-4}$	1.6	$1.8 \cdot 10^{-3}$	7.0	20	6.4	20
$\Delta u'v'_{3x8} \cdot 10^{-3}$	6.9	32	11	40	11	48	7.0	16	48
$\Delta u'v'_{3x10} \cdot 10^{-3}$	2.9	4.5	$4.4 \cdot 10^{-4}$	0.92	$8.1 \cdot 10^{-4}$	12	$2.8 \cdot 10^{-5}$	3.8	12
$\Delta u'v'_{3x11} \cdot 10^{-3}$	7.9	$2.8 \cdot 10^{-7}$	2.2	37	2.2	42	12	8.1	42
$\Delta u'v'_{3x15} \cdot 10^{-3}$	7.1	10	$9.8 \cdot 10^{-4}$	7.8	$3.5 \cdot 10^{-3}$	$5.4 \cdot 10^{-5}$	1.7	6.7	10
$\Delta u'v'_{3x16} \cdot 10^{-3}$	8.4	5.7	$5.9 \cdot 10^{-7}$	3.0	$4.1 \cdot 10^{-3}$	2.5	1.9	10	10
$\Delta u'v'_{3x17} \cdot 10^{-3}$	8.4	5.7	$5.9 \cdot 10^{-9}$	3.0	$4.1 \cdot 10^{-3}$	2.5	1.9	10	10
$\Delta u'v'_{3x19} \cdot 10^{-3}$	7.2	9.1	$3.6 \cdot 10^{-2}$	4.3	$3.6 \cdot 10^{-3}$	$9.3 \cdot 10^{-6}$	5.7	7.5	9.1
$\Delta u'v'_{3x20} \cdot 10^{-3}$	7.2	9.1	$3.6 \cdot 10^{-2}$	4.3	$3.6 \cdot 10 - 2$	$9.3 \cdot 10 - 6$	5.7	7.5	9.1
$\Delta u'v'_{3x22} \cdot 10^{-3}$	6.6	8.9	$4.8 \cdot 10^{-4}$	2.2	$1.8 \cdot 10^{-3}$	$2.3 \cdot 10 - 4$	3.2	7.2	8.9

Table 7: Optimum matrix (3 x 3) for the transformation RGB to XYZ as well as the formula for the calculation of the illuminance Ev from the RGB signals

E_v(lx) from R, G, B	$E_v = 683 \cdot (1.0001 \cdot E_{v,RGB} - 0.0066)$ (19) $E_{v,RGB} = 0.6802 \cdot R + 0.3651 \cdot G + 0.1751 \cdot B$ (20) $R^2 = 1.0$; $RMSE = 0.15$
Matrix 3 x 3 in case of the 9 light sources of training set	$\begin{pmatrix} 5.73 \cdot 10^5 & -4.17 \cdot 10^5 & -2.27 \cdot 10^5 \\ 3.64 \cdot 10^5 & -4.50 \cdot 10^4 & -3.26 \cdot 10^5 \\ -6.61 \cdot 10^4 & 2.04 \cdot 10^5 & 1.13 \cdot 10^6 \end{pmatrix}$ (21)

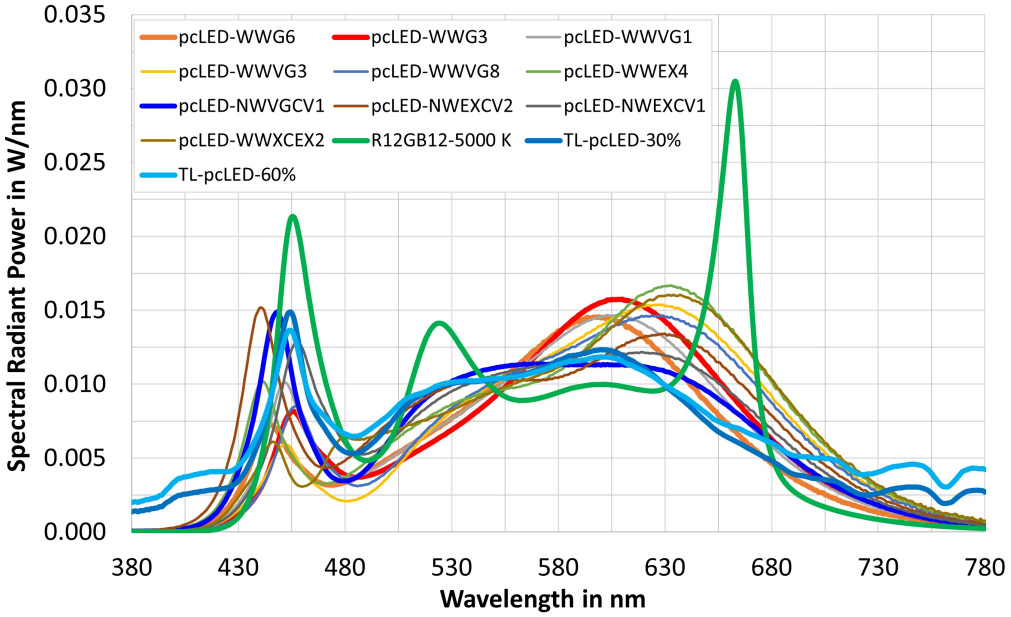

Figure 10. Lamp spectra of 13 light source types for the validation of the 3 x 3 matrix in Table 7.

.

often the case in practical indoor lighting (see Figure 10). The illuminance was again set to 750 lx. The results of the check are shown in Table 8. From Table 8 it can be seen that,

(a) The deviation of the illuminances, once calculated directly from the lamp spectra and once via the RGB color sensor signals and via the formula in Table 7, is below 0.65% in percentage terms;

Preprints (www.preprints.org) | NOT PEER-REVIEWED | Posted: 6 April 2023 doi:10.20944/preprints202304.0087.v1

(b) For the majority of pc-LEDs and for the combinations daylight-white LEDs, the chromaticity difference $\Delta u'v'$ is in a small or moderately small range from the point of view of practical lighting technology. An exception is the spectrum R12GB12-5000 K (green curve in Figure 10) with the three distinct peaks of the three RGB LEDs (B around 455 nm, G around 525 nm, R around 660 nm). There, the color difference is $\Delta u'v' = 10.1 \cdot 10^{-3}$.

For the case of daylight spectra a special matrix was found and described in Table 9. For the investigated RGB color sensor type, 185 daylight spectra were measured absolutely on a sunny summer day (August 19^{th}, 2020 in Darmstadt, Central Europe) from 6:32:00 in the early morning to 20:35:32 in the late evening. The chromaticity and illuminance values were calculated and used as a training set for the matrix. The largest color difference with a 3 x 3 matrix was found to be $\Delta u'v' = 1.2 \cdot 10^{-3}$ in the last minutes of the evening before sunset, when the correlated color temperature was very high, approximately in the range of 17000 K on the day of measurement. Most of the color differences were well below this value.

Table 8: Verification of optimal matrix (3 x 3) in Table 7 with 13 LEDs plus mixed daylight spectra

Name	pcLED-WWG6	pcLED-WWG3	pcLED-WWVG1	pcLED-WWVG3	pcLED-WWVG8	pcLED-WWEX4	pcLED-NWVG1	pcLED-NWEXCV2	pcLED-CWVG1	pcLED-CWEX2	R12GB12-5000 K	TL-pcLED-30%	TL-pcLED-60%
CCT (K)	3134	2801	3105	2782	2998	2969	4614	3942	5112	5059	5001	4391	4571
$CRI\ R_a$	80.27	84.06	85.63	88.10	90.56	94.41	90.91	93.09	90.06	95.99	89.73	89.85	92.48
x	0.4285	0.4434	0.4217	0.4557	0.4352	0.4252	0.3569	0.3764	0.3424	0.3439	0.3449	0.3644	0.3581
y	0.4025	0.3929	0.3841	0.4135	0.4003	0.3765	0.3608	0.3550	0.3537	0.3557	0.3495	0.3650	0.3605
E_v (lx)	750	750	750	750	750	750	750	750	750	750	750	750	750
$E_{v,new}$	750.35	752.29	752.54	750.90	751.14	754.17	751.40	754.79	751.31	750.01	747.60	751.94	751.91
x_{new}	0.4285	0.4434	0.4217	0.4557	0.4352	0.4252	0.3546	0.3779	0.3361	0.3368	0.3319	0.3665	0.3572
y_{new}	0.4025	0.3929	0.3841	0.4135	0.4003	0.3765	0.3643	0.3698	0.3545	0.3571	0.3529	0.3696	0.3640
$\Delta u'v' \cdot 10^{-3}$	$1.09 \cdot 10^{-7}$	$1.36 \cdot 10^{-7}$	$1.2 \cdot 10^{-7}$	$1.66 \cdot 10^{-7}$	$1.53 \cdot 10^{-7}$	$1.68 \cdot 10^{-7}$	3.15	8.76	4.5	5.32	10.1	2.42	2.51
ΔE_v in %	0.05	0.31	0.34	0.12	0.15	0.56	0.19	0.64	0.17	0.00	-0.32	0.26	0.25

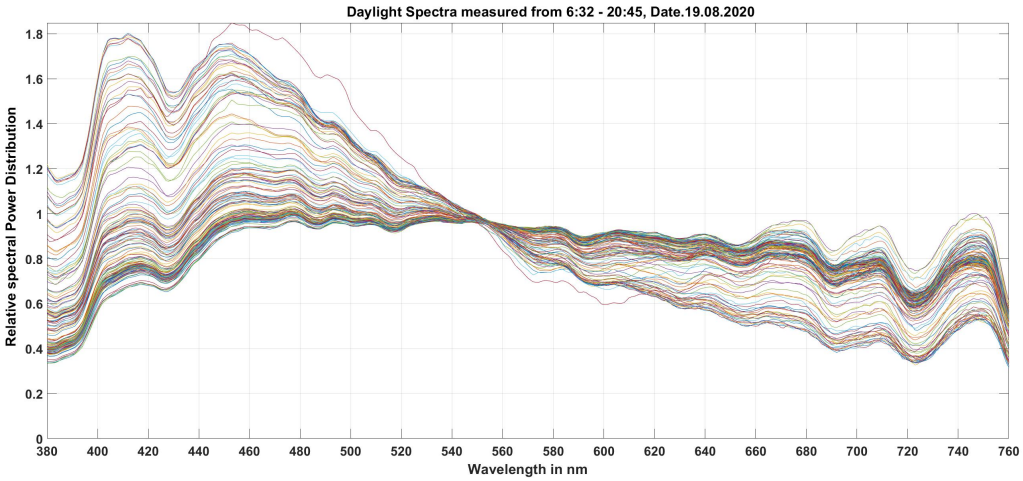

Figure 11. Some daylight spectra on a sunny day in Darmstadt, Germany (on August 19^{th}, 2020).

Table 9: Optimal matrix (3 x 3) for transforming RGB to XYZ and formula for calculating illuminance E_v from RGB signals in case of pure daylight.

E_v(lx) from R, G, B	$E_v = 683 \cdot (0.9987 \cdot E_{v,RGB} - 0.1124)$ (22) $E_{v,RGB} = 0.6333 \cdot R + 0.4804 \cdot G$ (23) $R^2 = 1.0;\ RMSE = 0.04$
Matrix 3 x 3 in the case of the 9 light sources of the training set	$\begin{pmatrix} 1.8558 & -1.6603 & 1.4322 \\ 1.1084 & -0.23047 & 0.53993 \\ 0.53135 & -0.97596 & 6.0956 \end{pmatrix}$ (24)

Preprints (www.preprints.org) | NOT PEER-REVIEWED | Posted: 6 April 2023 doi:10.20944/preprints202304.0087.v1

To verify the 3 x 3 matrix for daylight, 24 daylight spectra measured on a rainy day (September 23rd, 2020 in Darmstadt, Germany) were considered. The verification results are shown in Table 10 with 9 out of 24 spectra as examples. There the chromaticities and illuminances determined from the measured spectra are compared with the data obtained by matrixing the RGB color sensor (processed data). The calculated color difference $\Delta u'v'$ is very small and lies in the range of 10^{-4}.

Table 10: Verification of the 3 x 3 matrix for daylight spectra (trained on a sunny day, verified on a rainy day)

Sampling Time	07:27:17	10:03:31	11:06:01	12:03:19	13:05:50	14:07:40	15:10:10	16:12:41	19:14:58
CCT in K	12464	8033	6313	5651	5914	5853	5470	8174	16066
$E_{v,measure}$ in lx	401	9397	23940	58212	39463	43150	71006	15058	461
$x_{measusre}$	0.2652	0.2942	0.3163	0.3291	0.3236	0.3248	0.3332	0.2919	0.2568
$y_{measure}$	0.2831	0.3066	0.3293	0.3413	0.3364	0.3376	0.3449	0.3081	0.2705
$E_{v,processed}$ in lx	400.60	9403.02	23944.07	58205.57	39465.20	43149.59	70987.13	15070.62 4	60.41
$\Delta u'v'_{measure-calculate} \cdot 10^{-4}$	4.75	$2.81 \cdot 10^{-2}$	1.74	1.20	1.82	1.96	0.596	4.03	8.57

The determination of the optimal matrix for the transformation of RGB sensor signals into XYZ values and the illuminance E_v described so far, as well as the verification results with an actual RGB color sensor type, prove that it is possible to obtain the colorimetric and photometric values XYZ, E_v and CCT with relatively good results in the sense of a reliable, relatively accurate and adaptive lighting technology using inexpensive and commercially available color sensors. The next section deals with the accurate determination of the non-visual input quantities $mEDI$ and $mDER$ indoors (daylight and artificial light combined or separated) and outdoors during the day (with daylight only) from the tristimulus values XYZ and the illuminance E_v of a qualified RGB color sensor, because in practical lighting technology a spectroradiometer is often too expensive and too cumbersome to handle.

4. Prediction of a simple computational model of the non-visual quantities $mEDI$ and $mDER$ and verification of the feasibility of a RGB sensor using this model

Once the matrices for electric light sources and for daylight spectra have been optimized and found, the tristimulus values XYZ , the chromaticity coordinates xyz as well as the color temperature CCT and the illuminance E_v can be obtained from the RGB color sensors used (see the tables 7, 8, 9 and 10). To obtain the melanopic equivalent daylight illuminance $mEDI$, one only needs to know the value of $mDER$ and the illuminance E_v (in lx) according to equation 7, where the illuminance can be formed from the RGB signals (see formula in the tables 7 and 9) and is therefore determinable. Consequently, the most important task is to calculate the dimensionless input quantity $mDER$ (see Equation 9) from the chromaticity coordinates x, y, z (z turned out to be the most predictive, so it will be used).

Table 11: Measured and simulated spectra (4214 in total)

No.	Type of light sources and their parameter ranges CCT = 2201 – 17815 K; -1.467·10^{-2} < Duv < 1.529·10^{-2} 0.0797 < z < 0.4792; 80 < $CIE\ Ra$ < 100; 0.2784 < $MDER$ < 1.46
1.	Conventional incandescent lamps + filtered incandescent lamps
2.	Fluorescent tubes + Compact fluorescent lamps
3.	LED lamps + LED luminaires
4.	Daylight (CIE-model + measurements)
5.	Mixtures (DL+LED) - [mixture ratio = 10%-90%]
6.	Mixtures (DL+FL) - [mixture ratio = 10%-90%]

For this transformation from z to $mDER$, a large number of measured and simulated light source spectra were analyzed (see Table 11). The first 4 light source groups are real

Preprints (www.preprints.org) | NOT PEER-REVIEWED | Posted: 6 April 2023 doi:10.20944/preprints202304.0087.v1

measured light sources from thermal radiators (28 light sources), compact and linear fluorescent lamps (252 light sources), different LED configurations (419 light sources) and 185 measured daylight spectra. These 884 light source spectra are shown in Figure 12. In order to simulate the combination of daylight with white LEDs or daylight with white fluorescent lamps, which can correspond to the lighting conditions of interiors with white LEDs or white fluorescent lamps with windows over a longer period of use, the authors of this paper took 185 measured daylight spectra and mixed them with a market-typical white LED spectrum or with a typical fluorescent lamp spectrum in 9 different mixing ratios from 10% to 90%. This can be seen in Figure 13 for the case of combining daylight spectra with white LEDs. For the fluorescent lamps it is similar, so a graphical representation of the mixing spectra is omitted here. The 185 daylight spectra with 9 mixing ratios each result in 1665 simulated spectra each for LED and fluorescent lamps (185 x 9 = 1665).

Using the 4214 light source spectra summarized in Table 11, 4214 $mDER$ values and

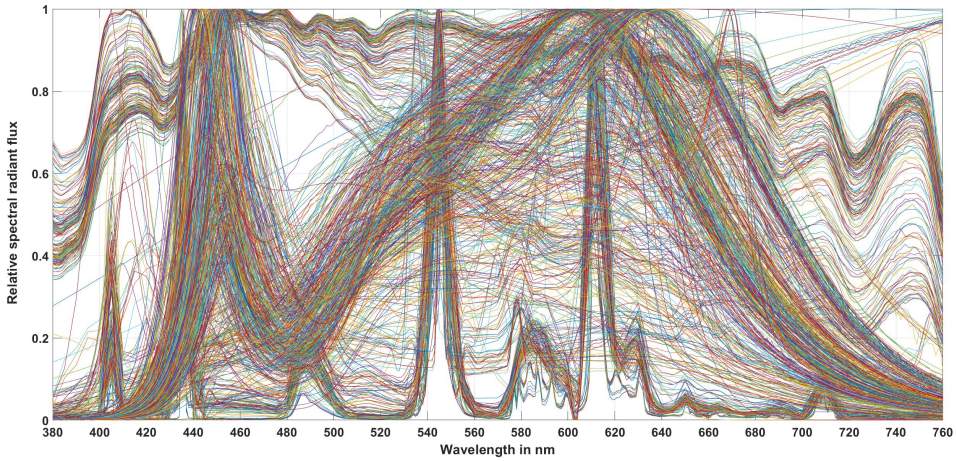

Figure 12. Spectra of 884 measured light source spectra.

4214 z values were calculated, from which their relation was determined. The formula for $mDER$ is given in Equation 25.

$$mDER = a \cdot e^{b \cdot z} - c \cdot e^{d \cdot z} \tag{25}$$

The parameters a, b, c and d for the fitting function and the correlation coefficients R^2 are given in Table 12. The course of the correlation between $mDER$ (ordinate) and the chromaticity coordinate z (abscissa) is shown in Figure 14, where the fitting function follows the green course of the curve.

Table 12: Parameter a, b, c and d for the fit function in Equation 25 and the correlation coefficient R^2

Parameter	a	b	c	d	R^2
Value	0.53806	2.3212	-0.37585	-0.85808	0.968

To check the predictive quality of Equation 25 and the transformation from z to $mDER$, the 4214 spectra in Table 11 were first used to calculate the 4214 $mDER$ values from the spectra themselves (denoted as $mEDR_{[CIES026/E:2018]}$) and then another 4214 $mDER$ values indirectly via Equation 25 with z as the independent variable (denoted as $mEDR = f(z)$), see Figure 15. The goodness of fit (R^2) was 0.97844, the linear constants are 1.0214 and -0.05712. Compared to the ideal constants of 1 and 0, the quality of the fit is very good.

Preprints (www.preprints.org) | NOT PEER-REVIEWED | Posted: 6 April 2023 doi:10.20944/preprints202304.0087.v1

To verify the quality of the characterization of the RGB color sensor under test (see

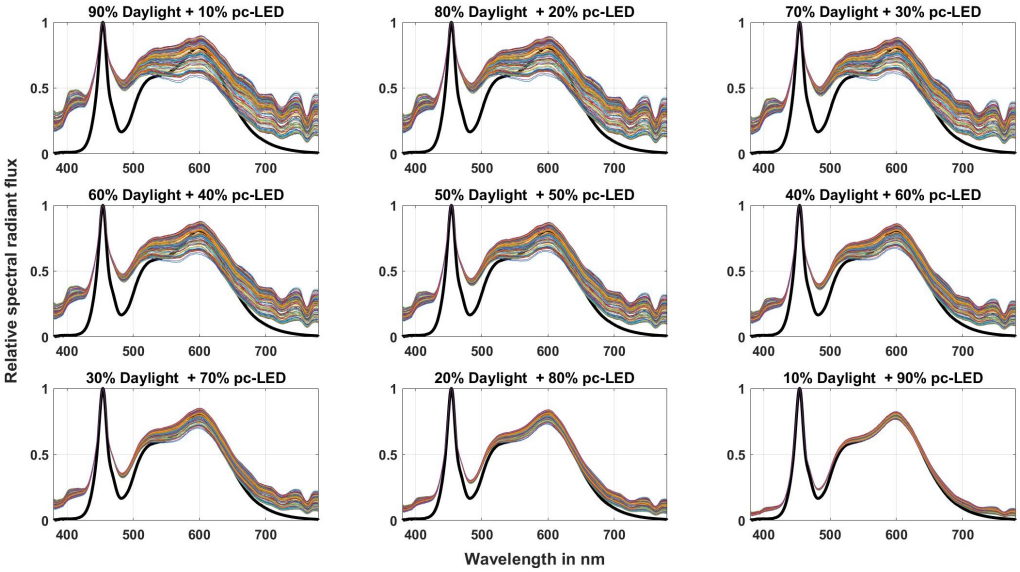

Figure 13. Spectra of 185 phases of daylight, mixed with white LEDs in 9 mixture ratios from 10% until 90%.

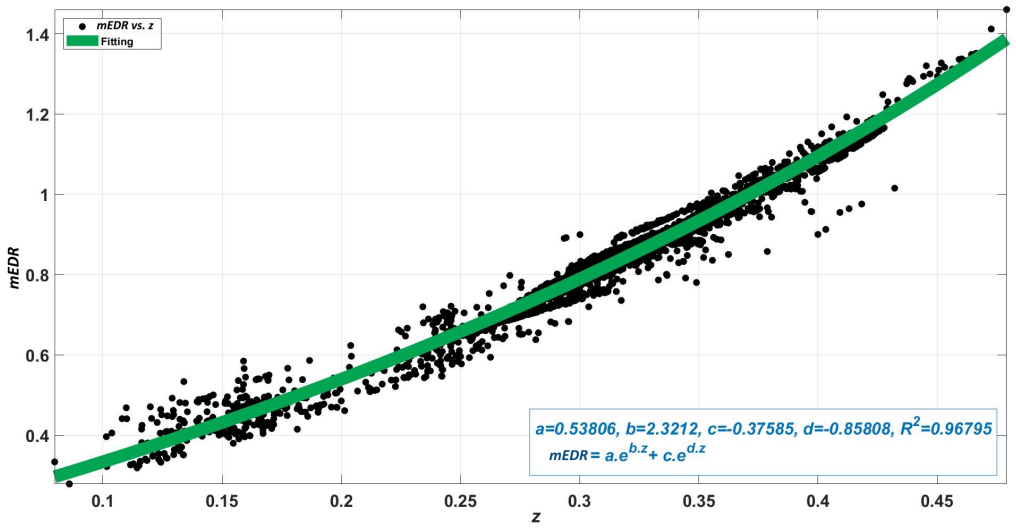

Figure 14. Correlation between $mDER$ (ordinate) and the chromaticity coordinate z (abscissa).

Figure 7), the quality of the "*matrixing*" in the transformation from RGB to XYZ and E_v (see Table 7) and the quality of the transformation from z to $mDER$ (see Equation 25) and finally the calculation of $mEDI$ (see the equations 6 and 9), we set each of the 13 light source spectra in Figure 10 to 750 lx. From these 13 spectra, the chromaticity coordinates x and y and the quantities CCT, CRI R_a, E_v, $mDER_{original}$, and $mEDI_{original}$ were calculated. They are listed in Table 13. For these 13 spectra, the chromaticity coordinates x_{new} and y_{new}, the value of $E_{v,new}$, and the values $mDER_{new}$ and $mEDI_{new}$ were also calculated from the RGB color sensor values by matrixing and transforming z to $mDER$ and $mEDI$, respectively. The maximum relative deviations $\Delta mDER$ (in %) and $\Delta mEDI$ (in %) were found to be in the range of ± 3.3%.

Preprints (www.preprints.org) | NOT PEER-REVIEWED | Posted: 6 April 2023 doi:10.20944/preprints202304.0087.v1

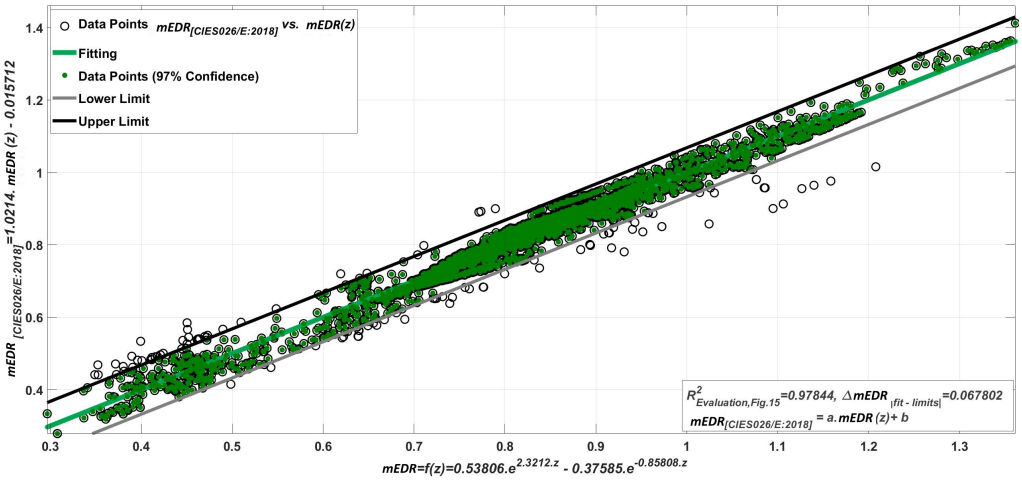

Figure 15. Comparison of the 4214 $mDER$ values on the ordinate, calculated from the spectra themselves (denoted as $mEDR_{[CIES026/E:2018]}$), with the 4214 $mDER$ $(= f(z))$ values calculated using Equation 25. $R^2 = 0.97844$, the linear constants $a = 1.0214$, $b = -0.015712$ compared to the ideal constants 1 and 0 and the $\Delta mEDR$ 97% confidence interval of 0.067802 shows a good quality.

5. Conclusion and Discussion

In indoor lighting technology, including daylight components during the day, the daily task is to evaluate the lighting systems after completion of the building or after reconstruction, to assess the photometric and colorimetric quality of the newly developed interior luminaires and, in the context of intelligent lighting (smart lighting, HCL lighting, integrative lighting), to adaptively control the lighting systems in order to provide the room users with the best visual and non-visual conditions and room atmosphere at all times. In addition to the criteria of visual performance according to current national and international standards (e.g. EN DIN 12464 [10]), aspects of psychological-emotional lighting effects as well as the evaluation and adaptive control of lighting systems according to non-visual quality characteristics should be considered. For this purpose, non-visual input parameters such as $mEDI$ and $mDER$ need to be measured and processed with sufficient accuracy, reliability and reasonable effort.

Existing illuminance meters, luminance meters, color and luminance cameras, and small portable colorimeters are currently only capable of measuring photometric quantities such as illuminance Ev, luminance L_v, colorimetric parameters such as chromaticity coordinates xyz, and correlated color temperature (CCT). To measure the non-visual parameters, a transformation is needed to convert the tristimulus values to the non-visual parameters, and a sensor platform is needed to convert the RGB sensor signals to the tristimulus values XYZ and E_v (in lx).

The authors of this paper have characterized some exemplary RGB color sensors on the basis of laboratory measurements, calculations and optimizations, by creating one or more matrices for optimal transformation of RGB sensor signals to the tristimulus values, and then, on the basis of extensive calculations, have achieved a transformation of the chromaticity coordinate z to $mDER$ and, via E_v, also to $mEDI$ with good accuracy. This work and the methodology described therein allow an accurate and financially justifiable assessment of lighting installations according to non-visual criteria, which will become increasingly important in the coming decades.

The goal of this paper was to provide a framework and a general methodology for using commercially available RGB sensors and qualifying them for measuring the met-

Preprints (www.preprints.org) | NOT PEER-REVIEWED | Posted: 6 April 2023 doi:10.20944/preprints202304.0087.v1

rics for non-visual effects. The results have some limitations because only one type of *RGB* sensor was used in this work. Other *RGB* sensor types may have different spectral, optical, and electronic characteristics with different dark currents, signal-to-noise ratios, and crosstalk effects, which should require different forms of matrices (e.g., matrices with higher-order *RGB* signals). Further studies are planned to compare the accuracies of several commercial *RGB* sensor types with the measurement results of an absolute spectroradiometer for different test conditions (e.g. outdoor and indoor lighting conditions with different mixing ratios of daylight and artificial light sources).

Table 13: Chromaticity difference $\Delta u'v'$ for different matrix types for the lamp types of the training set

Name	pcLED-WWG6	pcLED-WWG3	pcLED-WWVG1	pcLED-WWVG3	pcLED-WWVG8	pcLED-WWEX4	pcLED-NWVG1	pcLED-NWEXCV2	pcLED-CWVG1	pcLED-CWEX2	R12GB12-5000 K	TL-pcLED-30%	TL-pcLED-60%
CCT (K)	3134	2801	3105	2782	2998	2969	4614	3942	5112	5059	5001	4391	4571
CIE Ra	80.27	84.06	85.63	88.10	90.56	94.41	90.91	93.09	90.06	95.99	89.73	89.85	92.48
x	0.4285	0.4434	0.4217	0.4557	0.4352	0.4252	0.3569	0.3764	0.3424	0.3439	0.3449	0.3644	0.3581
y	0.4025	0.3929	0.3841	0.4135	0.4003	0.3765	0.3608	0.3550	0.3537	0.3557	0.3495	0.3650	0.3605
Ev (lx)	750	750	750	750	750	750	750	750	750	750	750	750	750
$mDER_{original}$	0.47	0.46	0.51	0.40	0.48	0.53	0.75	0.67	0.81	0.83	0.83	0.71	0.75
$mEDI_{original}$	349.06	347.67	383.55	300.60	358.27	395.93	562.91	500.06	610.69	625.10	625.79	532.40	563.22
$E_{v,new}$ (lx)	750.35	752.29	752.54	750.90	751.14	754.17	751.40	754.79	751.31	750.01	747.60	751.94	751.91
x_{new}	0.4285	0.4434	0.4217	0.4557	0.4352	0.4252	0.3546	0.3779	0.3361	0.3368	0.3319	0.3665	0.3572
y_{new}	0.4025	0.3929	0.3841	0.4135	0.4003	0.3765	0.3643	0.3698	0.3545	0.3571	0.3529	0.3696	0.3640
$mEDR_{new}$	0.47	0.46	0.53	0.39	0.46	0.54	0.74	0.66	0.82	0.81	0.83	0.69	0.73
$mEDI_{new}$	353.75	346.28	396.00	295.19	346.92	403.79	554.58	500.85	612.52	604.47	621.78	521.19	550.29
$\Delta u'v' \cdot 10^{-3}$	$1.09 \cdot 10^{-7}$	$1.36 \cdot 10^{-7}$	$1.20 \cdot 10^{-7}$	$1.66 \cdot 10^{-7}$	$1.53 \cdot 10^{-7}$	$1.68 \cdot 10^{-7}$	3.15	8.76	4.50	5.32	10.1	2.42	2.51
ΔE_v in %	0.05	0.31	0.34	0.12	0.15	0.56	0.19	0.64	0.17	0.00	-0.32	0.26	0.25
$\Delta mEDR$ in %	1.3	-0.7	2.9	-1.9	-3.3	1.4	-1.7	-0.5	0.1	-3.3	-0.3	-2.4	-2.5
$\Delta mEDI$ in %	1.35	0.40	3.25	1.80	3.17	1.99	1.48	0.16	0.30	3.30	0.64	2.10	2.30

Author Contributions: Conceptualization, V.Q.T., P.B. and T.Q.K.; Data curation, V.Q.T.; Formal analysis, V.Q.T., P.B.; Methodology, Q.V.T. and T.Q.K; Software, V.Q.T.; Supervision, T.Q.K.; Validation, V.Q.T and P.B.; Visualization, V.Q.T.; Writing—original draft, V.Q.T. and P.B.; Writing—review & editing, V.Q.T., P.B, and T.Q.K; Project administration, V.Q.T. All authors have read and agreed to the published version of the manuscript.

Funding: This work received no specific grant from any funding agency in the public, commercial, or not-for-profit sectors. The publication of the manuscript is supported by the Open Access Publishing Fund of the Technical University of Darmstadt.

Institutional Review Board Statement: Not applicable

Informed Consent Statement: Not applicable

Data Availability Statement: All data generated or analyzed to support the findings of the present study are included this article. The raw data can be obtained from the authors, upon reasonable request.

Conflicts of Interest: The authors declare no conflict of interest.

References

1. Commission International de l'Eclairage (CIE). CIE S 026/E: 2018: CIE System for Metrology of Optical Radiation for ipRGC-Influenced Responses to Light. *Vienna, Austria: CIE Central Bureau* **2018**. doi:10.25039/S026.2018.
2. Rea, M.S.; Ouellette, M.J. *Relative visual performance: A basis for application*; Vol. 23, SAGE Publications Sage UK: London, England, 1991; pp. 135–144. doi:10.1177/096032719102300301.
3. Rea, M.S.; Ouellette, M.J. Visual performance using reaction times. *Lighting Research & Technology* **1988**, *20*, 139–153. doi:10.1177/096032718802000401.
4. Weston, H.C.; others. The Relation between Illumination and Visual Efficiency-The Effect of Brightness Contrast. *The Relation between Illumination and Visual Efficiency-The Effect of Brightness Contrast.* **1945**.
5. Boyce, P.R. *Human factors in lighting*; Crc press, 2014. doi:10.1201/b16707.
6. Lindner, H. Beleuchtungsstärke und Arbeitsleistung–Systematik experimenteller Grundlagen (Illumination levels and work performance–systematic experimental principles). *Zeitschrift für die gesamte Hygiene und ihre Grenzgebiete (Journal of hygiene and related disciplines) 21* **1975**, pp. 101–107.
7. Schmidt-Clausen, H.J.; Finsterer, H. *Beleuchtung eines Arbeitsplatzes mit erhöhten Anforderungen im Bereich der Elektronik und Feinmechanik*; Wirtschaftsverl. NW, 1989.
8. Blackwell, H.R. Contrast thresholds of the human eye. *Josa* **1946**, *36*, 624–643.
9. Commission International de l'Eclairage (CIE). An analytical model for describing the influence of lighting parameters upon visual performance. *CIE-Publication* **1981**.

10. DIN-EN-12464-1-2021-11. Licht und Beleuchtung – Beleuchtung von Arbeitsstaetten, Teil 1: Arbeitsstaetten in Innenraeumen, 2021.
11. Houser, K.W.; Tiller, D.K.; Bernecker, C.A.; Mistrick, R. The subjective response to linear fluorescent direct/indirect lighting systems. *Lighting Research & Technology* **2002**, *34*, 243–260. doi:10.1191/1365782802li039oa.
12. Tops, M.; Tenner, A.; Van Den Beld, G.; Begemann, S. The effect of the length of continuous presence on the preferred illuminance in offices. Proceedings CIBSE Lighting Conference, 1998.
13. Juslén, H. *Lighting, productivity and preferred illuminances: field studies in the industrial environment*; Helsinki University of Technology Helsinki, 2007.
14. Moosmann, C. *Visueller Komfort und Tageslicht am Bueroarbeitsplatz: Eine Felduntersuchung in neun Gebaeuden*; KIT Scientific Publishing, 2015.
15. Park, B.C.; Chang, J.H.; Kim, Y.S.; Jeong, J.W.; Choi, A.S. A study on the subjective response for corrected colour temperature conditions in a specific space. *Indoor and Built Environment* **2010**, *19*, 623–637. doi:10.1177/1420326X10383472.
16. Lee, C.W.; Kim, J.H. Effect of LED lighting illuminance and correlated color temperature on working memory. *International Journal of Optics* **2020**, *2020*, 1–7. doi:10.1155/2020/3250364.
17. Fleischer, S.E. Die psychologische Wirkung veränderlicher Kunstlichtsituationen auf den Menschen. PhD thesis, ETH Zurich, 2001.
18. Khanh; T. Q.; Bodrogi, P.; Trinh, Q. V.. *Beleuchtung in Innenräumen – Human Centric Integrative Lighting Technologie, Wahrnehmung, nichtvisuelle Effekte*; Wiley-VCH (Verlag), 2022.
19. Lok, R.; Smolders, K.C.; Beersma, D.G.; de Kort, Y.A. Light, alertness, and alerting effects of white light: a literature overview. *Journal of biological rhythms* **2018**, *33*, 589–601. doi:10.1177/0748730418796443.
20. Souman, J.L.; Tinga, A.M.; Te Pas, S.F.; Van Ee, R.; Vlaskamp, B.N. Acute alerting effects of light: A systematic literature review. *Behavioural brain research* **2018**, *337*, 228–239. doi:10.1016/j.bbr.2017.09.016.
21. Dautovich, N.D.; Schreiber, D.R.; Imel, J.L.; Tighe, C.A.; Shoji, K.D.; Cyrus, J.; Bryant, N.; Lisech, A.; O'Brien, C.; Dzierzewski, J.M. A systematic review of the amount and timing of light in association with objective and subjective sleep outcomes in community-dwelling adults. *Sleep health* **2019**, *5*, 31–48. doi:10.1016/j.sleh.2018.09.006.
22. Commission International de l'Eclairage (CIE). User Guide to the α-opic Toolbox for implementing CIE S 026 **2020**. doi:10.25039/S026.2018.TB.
23. Brown, T.M.; Brainard, G.C.; Cajochen, C.; Czeisler, C.A.; Hanifin, J.P.; Lockley, S.W.; Lucas, R.J.; Münch, M.; O'Hagan, J.B.; Peirson, S.N.; others. Recommendations for daytime, evening, and nighttime indoor light exposure to best support physiology, sleep, and wakefulness in healthy adults. *PLoS biology* **2022**, *20*, e3001571. doi:journal.pbio.3001571.
24. ISO/CIE TR 21783:2022 | ISO/CIE TR 21783. Light and lighting - Integrative lighting - Non-visual effects, 2022.
25. Commission Internationale de l'Éclairage (CIE). Colourimetry, 2018.
26. Westland, S.; Ripamonti, C.; Cheung, V. *Computational colour science using MATLAB*; John Wiley & Sons, 2012.
27. Bieske, K. *Über die Wahrnehmung von Lichtfarbenänderungen zur Entwicklung dynamischer Beleuchtungssysteme*; Der Andere Verlag, 2010.